

Mixed valence nature of the Ce 4*f* state in CeCo₅ based on spin-polarized DFT+DMFT calculations

Ruiwen Xie* and Hongbin Zhang

Institute of Materials Science, Technical University of Darmstadt, Otto-Berndt-strasse 3, 64287 Darmstadt, Germany

(Received 10 July 2022; revised 2 December 2022; accepted 6 December 2022; published 13 December 2022)

Cerium-based intermetallics are currently attracting much attention as highly promising alternatives to conventional permanent magnets that contain a scarce rare earth element like neodymium. In the present work we apply a charge fully self-consistent approach combining density functional theory and dynamical mean-field theory (DFT + DMFT) to investigate the magnetization and electronic structure of the CeCo₅ system. We treat simultaneously the correlation effects in Ce-4*f* and Co-3*d* orbitals while taking the spin polarization into account. The calculated magnetic moment corresponding to the Ce-4*f* shell using the DFT + DMFT method is found to be drastically reduced as compared to the DFT results. Moreover, the Ce-4*f* valence state fluctuations are evaluated and compared within CeCo₅ and Ce(Co_{0.8}Cu_{0.2})₅ on account of the trivalent Ce in CeCu₅. Regarding the Cu substitutions at two Wyckoff positions of Co (2c and 3g), the substitution at 3g sites slightly enhances the magnetic moment of Ce while the substitution at 2c sites leads to nearly vanishing Ce and Co moments. Such a contrast may contribute to the experimentally reported nonmonotonic change of the magnetic anisotropy with increasing Cu alloying content in Ce(Co_{1-x}Cu_x)₅ alloys.

DOI: [10.1103/PhysRevB.106.224411](https://doi.org/10.1103/PhysRevB.106.224411)**I. INTRODUCTION**

High performance permanent magnets based on rare-earth (RE) and transition metal (TM) elements, e.g., Nd₂Fe₁₄B and SmCo₅, are promising for energy applications such as wind turbines and electric vehicles [1]. For these compounds, the localized 4*f* electrons of the RE elements give rise to a high magnetocrystalline anisotropy due to the nonspherical nature of the RE-4*f* charges caused by the crystal fields [2–4]. In addition, the magnetic moments of RE-4*f* and TM-3*d* states are coupled indirectly via the RE-5*d* orbitals, i.e., on-site spin moments originated from the RE-4*f* and RE-5*d* states couple ferromagnetically, whereas the spin moments derived from the RE-5*d* and TM-3*d* states are mostly antiferromagnetically coupled [5]. This leads to a complex problem of two coupled magnetic sublattices governed by hierarchical interactions [6] and hence a highly nontrivial subject to develop thorough understanding of the magnetic coercivity in 4*f*-3*d* intermetallics [7]. For instance, it is challenging to develop consistent theoretical description on the magnetic moment of RE ions beyond the atomic limits in order to guide the design of permanent magnets with optimal performance [8].

Driven by their potential application as high-performance permanent magnets, the prototypical RECo₅ series of compounds with the hexagonal CaCu₅-type structure have been under intensive investigation for over four decades [9–12]. In particular, the Ce-based RE-TM intermetallic compounds are highly attractive as Ce is more abundant in nature and less critical than Nd and Sm. On the other hand, in contrast to RECu₅ which follows lanthanide contraction with respect to the volume [13], the RECo₅ series see anomalies of CeCo₅

not only in lattice parameter, but also in magnetic moment and Curie temperature [10]. The anomaly in volume change is thought to be associated with the mix valence state of Ce in CeCo₅. Instead, the Ce in CeCu₅ is identified as trivalent with an antiferromagnetic lattice at around 4 K, and the shallow minimum in resistivity indicates the simultaneous presence of long-range magnetic order and Kondo effect [14]. Upon Cu doping into CeCo₅, the stability, magnetic coercivity and magnetic anisotropy are enhanced, which is usually ascribed to the transition from Ce⁴⁺ to Ce³⁺ valence state [15–17]. Experimentally, the valence state of Ce is usually derived from the combinations of magnetic properties and x-ray absorption spectroscopy (XAS) [18,19]. However, the quantification of the valence state is difficult due to both the electronic change in the Ce-4*f* shell and the presence of Ce oxide [19].

In the context of permanent magnets, the mix valence state of Ce-4*f* makes it problematic to obtain the magnetic anisotropy constant K_1 following $K_1 = -3J(J-1)\alpha_J\langle r^2 \rangle A_2^0 n_R$ based on the crystal field parameter A_2^0 [20,21], since there might be no 4*f* electrons for Ce⁴⁺. Moreover, it is essential to quantitatively evaluate the energy splitting between J multiplets, as well as the hybridization between 4*f* and other orbitals to determine the magnetic anisotropy [22]. It is also well-known that the Ce-4*f* electrons tend to form heavy-electron itinerant bands, as observed in the so-called “heavy-fermion” compounds [23,24], for instance, CeFe₂ Laves phase [25], Ce₂Fe₁₄B [26], and CeCo₅ [27]. For heavy fermions, the local magnetic moment of Ce is screened by conduction electrons, which significantly limits the magnetic hardness of Ce-TM intermetallics [25–27]. All these peculiar features of Ce-4*f* electrons cast unique yet complicated magnetic properties in Ce-TM intermetallics.

Thus, a question which arises is how to treat the strongly correlated Ce-4*f* electrons, which is beyond the commonly

*ruiwen.xie@tmm.tu-darmstadt.de

used approaches in the literature. A popular approach is the so-called “open core” scheme, in which the $4f$ states are removed from the valence band and treated as frozen in the core [28]. This method has been generalized to the spin-polarized open core approximation, applied for high-throughput design of permanent magnets [29]. The second approach is to use self-interaction correction (SIC), which can be a reasonable choice if the targeted states are fairly localized [7, 11, 30]. The third method is DFT + U [31], which is basically just a local Hartree-Fock approximation. All these methods suffer from the fact that only one Slater determinant is used, which is by nature not sufficient to get a proper description of the mixed valence state. In this regard, the dynamical mean-field theory (DMFT) method [32, 33] is capable of handling the local many-body problem and hence capturing the correlated nature of $4f$ shell. In the DMFT regime, the Hubbard-I approximation has been used as an impurity solver to tackle the magnetic properties of Ce-based intermetallic compounds, where the hybridization between Ce- $4f$ and other valence states is not explicitly considered [33, 34]. By contrast, the state-of-the-art continuous time quantum Monte Carlo (CTQMC) impurity solver can be used to quantify the valence states of the Ce- $4f$ shell [35].

In this work we performed systematic DFT + DMFT calculations on the CeCo₅ system with the correlation effects of Ce- $4f$ and Co- $3d$ orbitals consistently considered in the spin-polarized state. We demonstrate that not only the occupation (i.e., the valence state) of the $4f$ shell but also their spin polarization can be tailored by the hybridization function, which has significant influence on the resulting magnetic properties. Section II provides a detailed description of the employed DFT + DMFT method. The computational results are demonstrated in Sec. III. Starting with YCo₅ as a reference system (Sec. III A), we then investigate the magnetization at different temperatures (Sec. III B), the electronic structure (Sec. III C) and the distribution of Ce- $4f$ mix valence states in CeCo₅ and Cu-doped CeCo₅ structures (Sec. III D). The peculiar impact of Cu doping at different local chemical environments is discussed in Sec. IV.

II. METHODOLOGY

We used stationary and charge self-consistent implementation of DFT + DMFT [36–38], which is capable of simultaneously treating the strongly localized $4f$ electrons, spin-orbit coupling (SOC), and on-site Kondo screening effect. (The one-shot DFT + DMFT calculation was also employed in CeCo₅ for comparison, see the Supplemental Material (SM) [39] Sec. I for more details.) This approach has been successfully applied to address the physical origin of the $\alpha \rightarrow \gamma$ transition in Ce [40, 41]. For the DFT part, the Kohn-Sham orbitals were solved using the WIEN2k package implementing a full-potential linear augmented plane-wave formalism [42]. The generalized gradient approximation (GGA) with Perdew-Burke-Ernzerhof (PBE) functional was used in this work [43]. The cutoff $R_{\text{MT}}K_{\text{MAX}}$ was set to 7.0. The uniform kmesh of $9 \times 9 \times 10$ was adopted for the Brillouin zone integration. CTQMC was used as the impurity solver within the DMFT regime [35]. In CeCo₅, with its crystal structure demonstrated in Fig. 1, we treated both

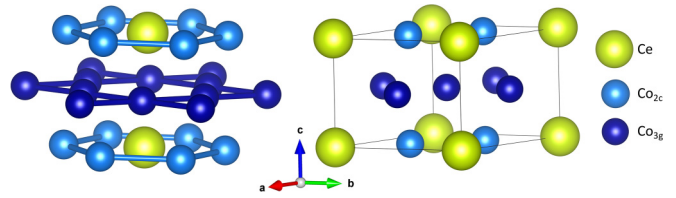


FIG. 1. Crystal structures of CeCo₅. The Ce and Co atoms are marked by yellow and blue colors, respectively. The Co_{2c} sites (light blue) are in plane with Ce while the Co_{3g} sites (dark blue) lie in between. This crystal structure fits for YCo₅ as well.

Ce- $4f$ and Co- $3d$ electrons as correlated. For Ce- $4f$ states, we considered a finite number of valences by including only $4f^0$, $4f^1$, $4f^2$, and $4f^3$ configurations. YCo₅ belongs to the same crystalline group as CeCo₅ and we considered the correlation effects of Co- $3d$ states in YCo₅. In addition, depending on the local crystal environments, we treated Co_{2c} and Co_{3g} as two different impurity sites. For the DMFT calculations, we chose real harmonics basis as the local basis of Co- $3d$ orbitals and the SOC is neglected for Co- $3d$ states. We used the $|j, m_j\rangle$ basis for the Ce- $4f$ shell since the SOC is significant in order to properly describe its physical properties. The spin polarizations of Co and Ce were introduced in the DMFT part by breaking the degeneracy of the spin-up and spin-down channels, and of the positive and negative j_z states, respectively. The direction of spin polarization is aligned along c ([001]) axis (see Fig. 1). The Coulomb interaction (U) and Hund’s exchange interaction (J) parameters corresponding to Ce- $4f$ and Co- $3d$ orbitals were properly tuned to fit reasonably with experimental magnetization. We employed the nominal double counting which was verified to be very close to exact double counting [44]. The comparisons among the nominal double counting, the fully localized limit, and the around mean-field schemes are demonstrated in the SM Sec. II [39]. The convergence criteria for charge and energy were $5 \times 10^{-6}e$ and 5×10^{-6} Ry, respectively. The number of Monte Carlo steps for each iteration is 9.6×10^7 . The density of states (DOS) was evaluated by implementing analytical continuations on the Matsubara self-energy functions $\Sigma(i\omega)$ [37] after the fully converged DFT + DMFT calculations with $\beta = 100$, equivalently at $T = 116$ K.

III. RESULTS

A. YCo₅ as the reference system

Taking YCo₅ as a benchmark ($a = 4.94$, $c = 3.98$ Å [45]), the spin moments of Co atoms obtained with various U and J values using the DFT + DMFT method are listed in the SM Sec. III, Table S1 [39]. The experimental values of spin moments of Co_{2c} and Co_{3g} at room temperature in Ref. [46] are 1.31 and 1.44 μ_B , respectively. Since the change of magnetization at low temperature range (≤ 300 K) is negligibly small [47], we select $U = 5.0$, $J = 1.1$ eV for correlated Co- $3d$ orbitals in all the following DFT + DMFT calculations at 116 K based on the obtained spin moments of YCo₅ (1.50 and 1.33 μ_B for Co_{2c} and Co_{3g}, respectively). The relatively larger U of Coulomb interaction parameter is due to the included on-site screening in the current DFT + DMFT scheme [48].

TABLE I. Decomposed moments of Ce and spin moments of Co. The DMFT results are obtained at $T = 116$ K. All quantities are in unit of μ_B . The available magnetic moments from previous work, including experiment and *ab initio* calculations, are listed for comparison.

	RE spin/orbital/total	Co _{2c} spin/orbital	Co _{3g} spin/orbital
YCo ₅			
DMFT	-/-/-	1.50/-	1.33/-
GGA	-0.20/-/-	1.57/-	1.59/-
GGA+SOC	-0.17/0.01/-0.16	1.59/0.12	1.61/0.11
GGA+U _{Co} +SOC	-0.19/0.06/-0.13	1.74/0.48	1.78/0.32
Expt. [46]	-/-/-	1.31/0.46	1.44/0.28
Calc. [47]	-	1.62/0.15	1.64/0.06
Calc. [49]	-	1.81/0.07	1.60/0.16
CeCo ₅			
DMFT	-0.10/0.32/0.22	1.30/-	1.21/-
GGA+U _{Ce} +SOC	-0.50/1.12/0.62	1.56/0.14	1.57/0.11
GGA+U _{Ce&Co} +SOC	-0.51/1.20/0.69	1.70/0.47	1.73/0.35
Calc. [33] (CeFe ₁₂)	-/-/0.27	-/-	-/-
Calc. [11]	-0.92/0.51/-0.41	7.19/1.14	
CeCo ₄ Cu _{2c}	-0.02/0.03/0.01	0.20/-	0.30/-
CeCo ₄ Cu _{3g}	-0.10/0.36/0.26	1.21/-	1.13/-

Note that the implementation of DMFT in combination with CTQMC is basis dependent, the orbital moment of Co is not considered in the applied real harmonics basis. Therefore, we compare with the experiment regarding only the spin moments of Co atoms in YCo₅ [46]. The obtained spin moments of Co in this work are in good agreement with the previously reported magnitudes of Co spins in YCo₅, as summarized in Table I [46,47,49].

Figure 2 shows the spin-resolved total DOSs of YCo₅ obtained using DFT and DFT + DMFT methods. The main changes of DOS, which are caused by including the correlation effects in the DFT + DMFT, are the broadening of spectra and the appearance of tails in the high binding energies (e.g.,

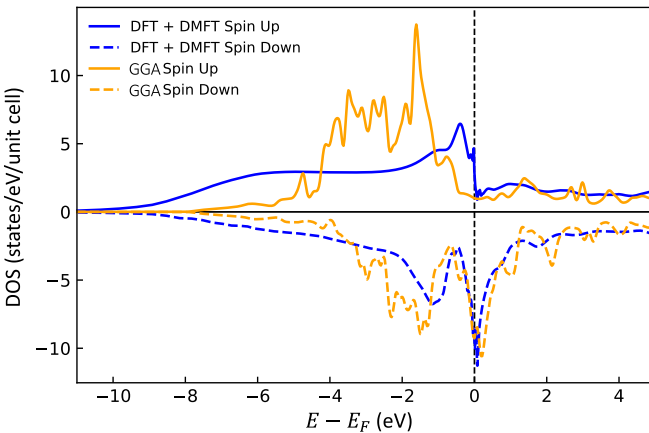


FIG. 2. Spin-polarized total density of states (DOS) of YCo₅. Solid and dashed lines are for majority and minority spin channels, respectively. Blue and orange colors represent the DFT + DMFT and DFT results, respectively.

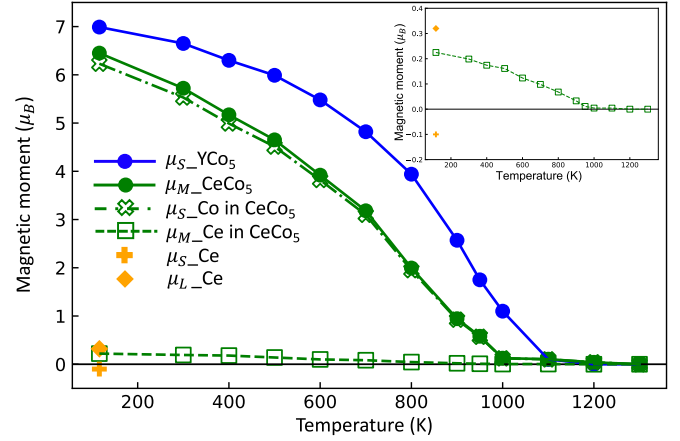


FIG. 3. Temperature dependence of total spin moment of YCo₅ (μ_S , blue solid line) and total magnetization of CeCo₅ (μ_M , green solid line). The temperature dependence of magnetization of Co and Ce in CeCo₅ are shown separately. The orbital moment of Co is not considered in the current work. μ_S denotes the total spin moment of Co. For Ce, its spin moment μ_S and orbital moment μ_L at $T = 116$ K are marked out. μ_M denotes its total magnetic moment. The inset zooms in the total magnetization of Ce versus temperature.

6 eV below the Fermi energy). Such differences between the DFT and DFT + DMFT results are consistent with previous observations [50]. In addition, the enhanced renormalization of the spin-up bands around E_F and the downshift of the bands around -6 eV can be clearly seen by comparing the DFT and DFT + DMFT spectral functions (see the SM Sec. IV, Fig. S3 [39]). By contrast, the minority spin channel is less influenced by the inclusion of correlation effects as compared to the majority spin channel. Such spin-dependent correlation effects have been detected in spin- and angle-resolved photoemission experiments for ferromagnetic transition metals Fe, Co, and Ni [51].

B. Magnetization with temperature

The magnetic moments versus temperature for YCo₅ obtained using the DFT + DMFT method are displayed in Fig. 3. The critical magnetic order transition temperature of YCo₅ is evaluated to be approximately 1100 K, which is slightly overestimated compared to the experimental value (987 K) [52]. This can be attributed to the fact that nonlocal transversal spin excitations are not considered in the DMFT calculations. We would also like to stress that in the present DFT + DMFT calculations, the Coulomb interaction is expressed using the rotationally invariant form, whereas the Ising approximation (i.e., density-density terms only) would lead to a much higher transition temperature and a larger magnetic moment as demonstrated for bcc Fe in Refs. [53,54].

The magnetic moments with respect to temperature for CeCo₅ ($a = 4.93$, $c = 4.02$ Å [55]) are also plotted in Fig. 3, where $U = 5.0$, $J = 1.1$ eV are adopted for the Co-3*d* orbitals, and $U = 7.0$, $J = 0.7$ eV for the Ce-4*f* orbitals. For the light rare-earth elements, the Hubbard U values ranging from 4 to 7 eV do not affect much the physical properties [56]. The calculated magnetic transition temperature of CeCo₅ is around 1000 K in comparison to the experimental value of 737 K [52].

As comparative cases, the GGA + U + SOC calculations for CeCo₅ using the WIEN2k package were also adopted by applying U only on Ce-4*f* states ($U = 7.0$ eV and $J = 0.8$ eV, denoted as GGA + U_{Ce} + SOC) and applying U and J on both Ce-4*f* ($U = 7.0$ eV and $J = 0.8$ eV) and Co-3*d* states ($U = 2.0$ eV and $J = 0.8$ eV, denoted as GGA + $U_{\text{Ce\&Co}}$ + SOC). The obtained magnetic moments of CeCo₅ are listed in Table I. The application of U on Co-3*d* orbitals increases its orbital moment significantly, as can be observed in the case of YCo₅ as well. Although the enhanced orbital moments of Co seem to fit better with experimental values [46], the calculated spin moments are much higher than the experimental results. Instead, the orbital polarization correction on top of the DFT method results in enhanced orbital moment and simultaneously negligible change of the spin moment [57,58]. However, as demonstrated later in our work, it is believed that the spin moments of Co atoms play a more essential role in the total magnetization of CeCo₅, thus we prefer to focus on the GGA + SOC results for Co atoms.

The GGA + U_{Ce} + SOC calculation gives spin and orbital moments of -0.50 and $1.12 \mu_B$ for Ce, respectively. The spin and orbital moments of Co_{2c} (Co_{3g}) are 1.56 (1.57) and 0.14 (0.11) μ_B , respectively (see Table I). The spin moments of Co_{2c} and Co_{3g} atoms calculated using the DFT + DMFT method are about 1.30 and $1.21 \mu_B$, respectively, which are slightly lower than the GGA + U_{Ce} + SOC results. Here we are more interested in comparing the spin and orbital moments of Ce obtained using the GGA + U_{Ce} + SOC and DFT + DMFT approaches. One apparent difference is that the GGA + U_{Ce} + SOC results show larger magnitudes of both the spin and orbital moments for Ce, i.e., $\mu_S = -0.50$ and $\mu_L = 1.12 \mu_B$ as given by the GGA + U_{Ce} + SOC, in comparison to $\mu_S = -0.10$ and $\mu_L = 0.32 \mu_B$ as obtained using the DFT + DMFT. According to Hund's rules, the spin angular momentum S of the Ce-4*f*¹ shell is equal to $1/2$ and the orbital angular momentum $L = 3$, resulting in the total angular momentum $J = |L - S| = 5/2$. For the Ce-4*f*¹ $J = 5/2$ shell, the gyromagnetic ratio g_J is $6/7$ and consequently the saturated Russel-Saunders value M_z should be equal to $g_J J = 2.14 \mu_B$. The magnitude of the total magnetic moment obtained using the DFT + DMFT method is well below the saturated Russel-Saunders value, which can be attributed to the Kondo screening effect [33]. Besides, we suspect that the mix valence states of Ce-4*f* shell also contribute to the reduced magnetic moment, which will be discussed in detail in Sec. III D. Additionally, as listed in Table I, the obtained Ce-4*f* moments using the DFT + DMFT are smaller than those given by the SIC approach [11], but are in good agreement with the magnetic moments of Ce in CeFe₁₂ calculated using also the DMFT method [33], suggesting that the local spin excitations can effectively reduce the magnitude of the magnetic moment.

C. Density of states of CeCo₅

The orbital-resolved DOSs for both Ce-4*f* and Co-3*d* states calculated using the GGA + U_{Ce} + SOC and DFT + DMFT approaches are shown Fig. 4. Similar to the case of YCo₅, the Co-3*d* DOS given by the DFT + DMFT method is broadened [Fig. 4(b)] as compared to that obtained using

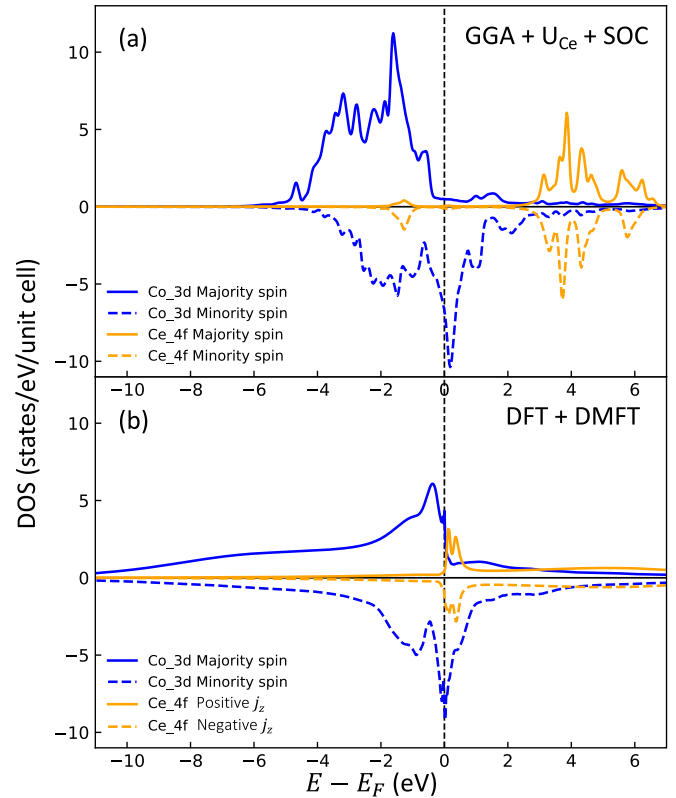


FIG. 4. Orbital-resolved and spin-polarized density of states of CeCo₅ obtained by using (a) WIEN2k (GGA + U_{Ce} + SOC) and (b) DFT + DMFT approaches.

the GGA + U_{Ce} + SOC method [Fig. 4(a)]. Moreover, the spin-dependent electronic correlations can be noticed as for Co in YCo₅. More noticeably, the positions of Ce-4*f* states given by the GGA + U_{Ce} + SOC and DFT + DMFT calculations are in stark contrast. The inclusion of static U in Ce-4*f* shell splits the occupied and unoccupied states [59], thus the unoccupied Ce-4*f* states are centered around 3.8 eV and the occupied Ce-4*f* states are located at approximately -1.3 eV in the GGA + U_{Ce} + SOC calculations, whereas the Ce-4*f* quasiparticle peaks are located near E_F in the DFT + DMFT picture, as indicated by the DOS (Fig. 4) and the spectral functions (see the SM Sec. IV, Fig. S4 [39]).

Such behaviors of the Ce-4*f* spectral functions can be confirmed by comparing to the experimental photoemission spectra, as shown in Fig. 5. The experimentally measured inverse photoemission spectroscopy, i.e., Bremsstrahlung isochromat spectroscopy (BIS) spectrum [61], together with the x-ray photoemission spectroscopy (XPS) spectrum [60] (see the inset of Fig. 5) are displayed in Fig. 5. Assuming Ce with one 4*f* electron, the XPS spectrum corresponds to $f^1 \rightarrow f^0$ transition while the BIS spectrum corresponds to $f^1 \rightarrow f^2$ transition. We can see from the experimental BIS spectrum that the Ce's f^1 and f^2 configurations are located at about 0.7 and 5.5 eV above the Fermi level, respectively. The positions of f^1 and f^2 of Ce according to the DFT + DMFT calculations (around 0.4 and 5.2 eV, respectively) agree well with the experimental observations. We can also note that the calculated Ce-4*f* spectra show a double-peak

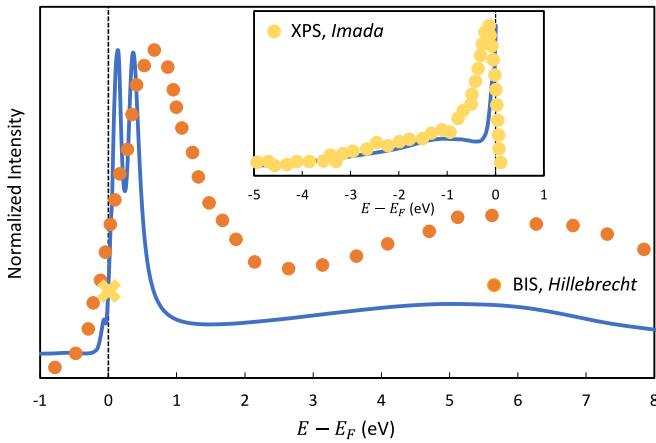


FIG. 5. Calculated spectra of Ce-4*f* orbitals in CeCo₅ using DFT + DMFT at 116 K (solid line), in comparison to experimental XPS [60] (yellow dots, see inset) and BIS [61] (orange dots) photoemission spectra. The black dashed line sits at E_F . The experimental data are normalized so that the intensity peak value from experiment is the same as that from DFT + DMFT calculations.

feature, which is attributed to the splitting of Ce-4*f* states to $j = 5/2$ and $j = 7/2$ caused by SOC. However, this double-peak feature is not revealed by the experimental BIS spectrum. Such difference can be understood from two main aspects. First, the unoccupied Co-3*d* states in the spin-down channel are still quite abundant in the energy range of 0–1 eV above the Fermi level [see Fig. 4(b)]. In other words, the contribution from the unoccupied Co-3*d* states to the BIS spectrum is not negligible anymore and results in the broadening of the BIS spectrum as compared to the DMFT calculations. The similar mechanism plays a role in the XPS spectrum as well. According to Ref. [60], most of Ce-4*f* and Co-3*d* intensities of CeCo₅ are distributed in the binding energy region of 0–3 eV. Especially for Ce-4*f* states, the binding energy is concentrated on a region of 0–1 eV, which is also confirmed by the DMFT calculation. The strongly mixed bands of Ce-4*f* and Co-3*d* characters are thus expected to exist when $E - E_F \in [-1, 0]$ eV. From the inset of Fig. 5, one can see the relatively larger difference between the experimental XPS spectrum and the calculated Ce-4*f* DOS at a binding energy range of 0–1 eV, while for binding energy larger than 1 eV where the band mixing is believed to play a negligible role, better agreement is observed. Besides the band mixing effect, the second reason for the absence of the double-peak feature in the BIS spectrum can be attributed to the limitations in the experimental instrument. As described in Ref. [61], the BIS spectrometer used in their work had an energy spread of 0.26 eV and the estimated total resolution was about 0.65 eV. In contrast, the energy difference between the $j = 5/2$ and $j = 7/2$ branches in the calculated spectrum is only around 0.28 eV, which is close to the instrumental energy spread and even smaller than the resolution. Therefore, if we consider the extra broadening caused by the experimental instrument, it is highly possible that the double-peak feature revealed in the DFT + DMFT calculations would be smeared out. Here we would like to stress that the focus is mainly the comparison regarding the positions corresponding to differ-

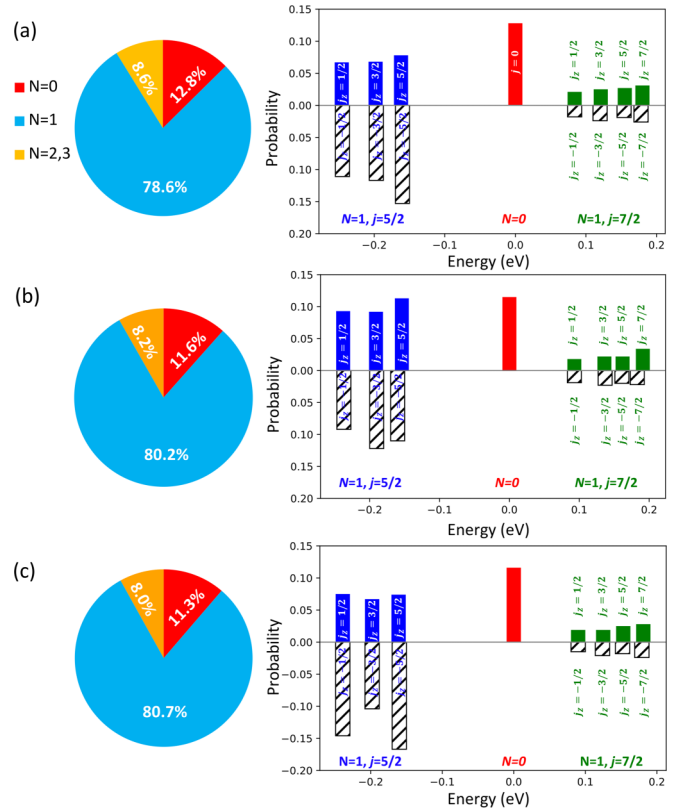


FIG. 6. Distributions of Ce-4*f* occupancy numbers (left panel with pie chart) and probabilities of Ce atomic eigenstates (right panel with histograms) in (a) CeCo₅, (b) CeCo₄Cu_{2c}, and (c) CeCo₄Cu_{3g}, respectively. The probabilities for positive and negative j_z are demonstrated in the upper and lower parts of the histograms, respectively.

ent Ce-4*f* configurations. In this regard, the DFT + DMFT method successfully evaluates the positions of Ce-4*f* intensity peaks and indicates the significance of incorporating dynamic hybridization between the 4*f* shell and its surroundings.

D. Impact of Cu substitution

To investigate the role of Cu in modifying the Ce-4*f* valence state, we further performed DFT + DMFT calculations on the Cu-doped CeCo₅ at $T = 116$ K. This is because the occupation probabilities of the atomic multiplets can be directly obtained in the current DFT + DMFT calculations and hence we are allowed to quantify the subtle electronic structure of the strongly correlated systems [62–64]. Correspondingly, the distributions of the Ce-4*f* occupancy numbers and the probabilities of Ce atomic eigenstates are illustrated in Fig. 6 for CeCo₅, CeCo₄Cu_{2c}, and CeCo₄Cu_{3g} systems, where the Cu atoms substitute Co_{2c} and Co_{3g} sites in CeCo₄Cu_{2c} and CeCo₄Cu_{3g}, respectively.

In the presence of SOC, the eigenstates of 4*f* shell are represented by good quantum numbers N (total occupancy), j (total angular momentum), and j_z . Here we truncate the states with $N > 3$, which possess negligible probabilities. As can be seen from Fig. 6, the probabilities of Ce-4*f* occupancies corresponding to $N = 0$ and $N = 1$ in CeCo₅ are 12.8% and 78.6%, respectively. The occupancy probability 12.8% of 4*f*⁰

agrees quite well with the deduced $4f^0$ weight for CeCo_5 of around 13.0% from the core-level XPS measurements based on the Anderson impurity model [65]. With Cu substituting the Co_{2c} and Co_{3g} sites, the probabilities of $N = 0$ are slightly reduced to 11.6% and 11.3%, respectively. As a consequence, the occupancy probability corresponding to $N = 1$ is slightly increased with Cu substitution. This trend is consistent with the conclusion drawn from the XPS of $\text{Ce}(\text{Co}_{1-x}\text{Cu}_x)_5$: [17] with increasing Cu content, the I_{4f^0}/I_{4f^1} absorption intensity peak ratio is reduced. Moreover, we have also employed a DFT + DMFT calculation for paramagnetic CeCu_5 and obtained nearly pure $4f^1$ configuration with negligible probability of $4f^0$ being around 1.6%.

Furthermore, as shown in the right panels of Fig. 6, the occupation probabilities of the $|\frac{5}{2}, \pm\frac{5}{2}\rangle$, $|\frac{5}{2}, \pm\frac{3}{2}\rangle$, $|\frac{5}{2}, \pm\frac{1}{2}\rangle$, $|\frac{7}{2}, \pm\frac{7}{2}\rangle$, $|\frac{7}{2}, \pm\frac{5}{2}\rangle$, $|\frac{7}{2}, \pm\frac{3}{2}\rangle$, and $|\frac{7}{2}, \pm\frac{1}{2}\rangle$ states are explicitly plotted. It is obvious that the spin and orbital moments of Ce atoms origin mainly from the $j = \frac{5}{2}$ states for pristine CeCo_5 [Fig. 6(a)]. The Cu doping remarkably alters the polarization of the $j = \frac{5}{2}$ states, i.e., the relative occupation of Ce- $4f$ states with positive and negative j_z values. For instance, with Cu substituting the Co_{2c} sites, the magnetic moment of Ce almost vanishes. By contrast, when Cu substitutes the Co_{3g} sites, the probabilities of $|\frac{5}{2}, -\frac{5}{2}\rangle$, $|\frac{5}{2}, -\frac{3}{2}\rangle$, and $|\frac{5}{2}, -\frac{1}{2}\rangle$ are apparently higher than that of $|\frac{5}{2}, \frac{5}{2}\rangle$, $|\frac{5}{2}, \frac{3}{2}\rangle$, and $|\frac{5}{2}, \frac{1}{2}\rangle$ states. Note that the $4f^0$ configuration does not contribute to magnetization, hence the reduced probability of $4f^0$ state in Cu-doped CeCo_5 systems should also slightly improve the magnetic moment of Ce. As a consequence, the total magnetic moment corresponding to the Ce- $4f$ shell in $\text{CeCo}_4\text{Cu}_{3g}$ is around $0.26 \mu_B$, which is also slightly higher than that in pristine CeCo_5 ($0.22 \mu_B$) (see Table I). In addition, the local spin moments of Co show remarkably differences in $\text{CeCo}_4\text{Cu}_{2c}$ and $\text{CeCo}_4\text{Cu}_{3g}$. The spin moments of Co_{2c} and Co_{3g} in $\text{CeCo}_4\text{Cu}_{2c}$ are 0.20 and $0.30 \mu_B$, respectively, while in $\text{CeCo}_4\text{Cu}_{3g}$ they are 1.21 and $1.13 \mu_B$, respectively (see Table I). Compared to the local spin moments of 1.30 and $1.21 \mu_B$ for Co_{2c} and Co_{3g} in CeCo_5 , the total magnetization (with Co orbital moment excluded as mentioned before) in $\text{CeCo}_4\text{Cu}_{2c}$ is drastically suppressed. Notice that we applied the same U and J sets in CeCo_5 , $\text{CeCo}_4\text{Cu}_{2c}$, and $\text{CeCo}_4\text{Cu}_{3g}$ systems.

In order to understand the difference in the total magnetization between $\text{CeCo}_4\text{Cu}_{2c}$ and $\text{CeCo}_4\text{Cu}_{3g}$ structures, we show in Fig. 7 the impurity hybridization functions of the Ce- $4f$ states in CeCo_5 , $\text{CeCo}_4\text{Cu}_{2c}$, and $\text{CeCo}_4\text{Cu}_{3g}$, respectively. We find that the Cu substitution introduces an extra hybridization peak at around -3.5 eV, regardless of the substitution sites. Except for this extra peak, the hybridization functions of Ce in $\text{CeCo}_4\text{Cu}_{3g}$ exhibit a similar pattern to those in pure CeCo_5 . However, when Cu occupies the Co_{2c} sites, the hybridization peak becomes significantly stronger both at around -3.5 eV and in the affinity of Fermi level. Namely, under the same adopted U and J values, Cu at the $2c$ sites introduces a stronger screening effect than that at the $3g$ sites, which explains the contrasting changes in the j_z occupation probabilities, and thus leads to the significantly reduced total magnetization in the Ce- $4f$ shell of $\text{CeCo}_4\text{Cu}_{2c}$.

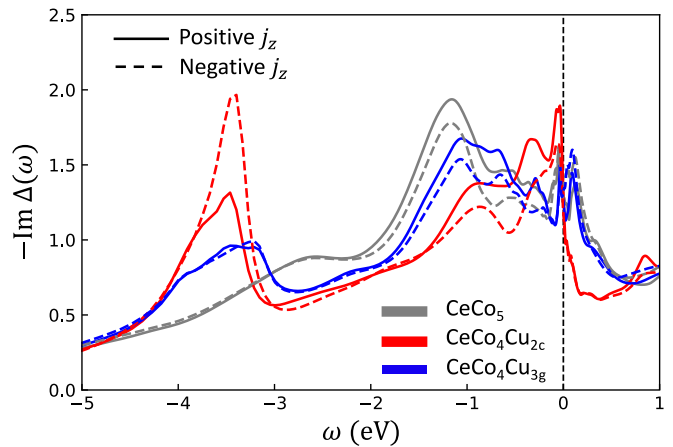


FIG. 7. Hybridization functions of Ce- $4f$ orbitals in CeCo_5 (gray line), $\text{CeCo}_4\text{Cu}_{2c}$ (red line), and $\text{CeCo}_4\text{Cu}_{3g}$ (blue line), respectively. For Ce- $4f$ states, the solid line and dashed line represent the hybridization function corresponding to positive and negative j_z , respectively.

IV. DISCUSSIONS

In the literature which have carried out *ab initio* calculations on ferro/ferrimagnetic RE-TM based systems, the correlation effects were either treated using the DFT + U method [59], or that the magnetism of TM is handled within the local spin-density approximation while only the RE- $4f$ shell is treated within the DMFT-QMC [33]. The present work considers simultaneously the dynamic correlation effects of Ce- $4f$ and Co- $3d$ orbitals and successfully converges to the antiparallel spin alignment between the two magnetic lattices. On the contrary, the direction of the total magnetization aligns parallel, as the orbital moment of Ce is greater than its spin moment.

According to the results demonstrated in Sec. III D, we find that when Cu substitutes one of the Co_{2c} sites in the unit cell, the magnetic moments of Ce and the remaining Co atoms are strongly reduced. By strong contrast, the Cu substitution at the Co_{3g} sites hardly affects the spin moments of the other Co atoms and the magnetic moment of Ce is slightly enhanced. Here we would like to stress that if we replace separately Co_{2c} and Co_{3g} with Cu in YCo_5 , the magnetization suppression as shown in $\text{CeCo}_4\text{Cu}_{2c}$ is not observed, indicating a close correlation between the magnetization reduction and the presence of correlated Ce- $4f$ electrons. Referring to the work in Ref. [17], we postulate that the Cu substitution at the $2c$ sites enhances the screening to the Ce- $4f$ moments, which would further block the spin exchange among Ce and Co atoms. Moreover, the neutron scattering indicated that the Co moments on the $3g$ sites are induced by an exchange field from that on the $2c$ sites in ThCo_5 and CeCo_5 [66,67]. Therefore, it is not surprising that the Cu doping at the $2c$ sites not only reduces the moment of Co_{2c} but also that of Co_{3g} .

The impact of Cu doping on the magnetic anisotropy energy (MAE) is also of great interest [59,68]. Unfortunately, calculating MAE using the DFT + DMFT approach for CeCo_5 and the Cu-doped systems is not realistic owing to the following reasons. On the one hand, the saturation magnetization of CeCo_5 along the hard axis is smaller than that along

the easy axis by 12% even under a high external magnetic field larger than 33 T [27], indicating that there still exists an angle between the Ce/Co moments and the hard magnetization axis. Moreover, for 4f-3d intermetallics, the single-ion MAE and the intersublattice magnetic exchange energy are of the same order, thus the alignments of 4f and 3d moments do not simply correspond to a (anti-)parallel configuration when the external magnetic field is along the hard axis [69]. Therefore, which magnetic configuration should be employed to simulate the condition with magnetization along the hard axis remains questionable [70]. On the other hand, SOC needs to be taken into account also for Co in the calculation of MAE under the framework of DFT + DMFT, which introduces off-diagonal components in the basis used in the CTQMC impurity solver and thus leads to a more severe sign problem. Despite the sign problem, the calculation of MAE requires high accuracy regarding the energy convergence, i.e., 1×10^{-7} eV at least, together with the employment of a high density of k mesh. With such criteria, the DFT + DMFT calculation would be too expensive. We are also aware that the MAE of YCo₅ has been calculated by Zhu *et al.* using the charge self-consistent LDA + DMFT approach [71], in which the spin-polarized T -matrix fluctuation (SPTF) exchange approximation technique was adopted as the impurity solver. However, from a physical point of view, the reliability of the calculated MAE for Ce-transition metal intermetallics using this approach is doubtful since SPTF properly depicted the bandlike features at and around the Fermi level of Ce-4f states in CeN but the multiplet structure, especially the peak corresponding to 4f² configuration, was missing [72].

Based on the discussions above, we speculate the effect of Cu doping on the magnetic anisotropy according to the current DFT + DMFT results. At low temperatures, the single-ion anisotropy of Ce is the main contribution to the first-order anisotropy constant (K_1) [27]. The Kondo screening is found to be larger when Cu substitutes the Co_{2c} site, leading to the huge magnetization reduction which is not favored by high MAE. In addition, among the $j = 5/2$ manifold, $|\pm 5/2\rangle$ states have the largest $|M_z|$, for which an easy-axis magnetic anisotropy is expected, while the $|\pm 1/2\rangle$ states correspond to an easy-plane anisotropy in the quasi-atomic picture. By comparing the occupations of the states in the Ce-4f $j = 5/2$ manifold among CeCo₅, CeCo₄Cu_{2c}, and CeCo₄Cu_{3g}, we found that Ce in CeCo₄Cu_{3g} possesses the largest occupation number corresponding to $|-5/2\rangle$ of around 0.19, as compared to that of 0.17 and 0.11 in CeCo₅ and CeCo₄Cu_{2c}, respectively. Regarding the $|+5/2\rangle$ state, the occupation number is 0.09, 0.14, and 0.09 in CeCo₅, CeCo₄Cu_{2c}, and CeCo₄Cu_{3g}, respectively. Therefore, we postulate that CeCo₄Cu_{3g} possesses larger magnetic anisotropy than both CeCo₅ and CeCo₄Cu_{2c} at low temperatures.

However, the contribution to the magnetic anisotropy from Ce-4f states is dominant at low temperature and overruled by transition metals close to room temperature [33]. According to the theoretical calculations of Okumura *et al.* [73], with Co atoms at 3g sites fully occupied by Cu in YCo₅, the uniaxial magnetic anisotropy of YCo₅ persists and its corresponding magnetic anisotropy energy is larger than that of YCo₅. Such results indicate that the magnetic interaction within the atomic layer containing the 2c sites is the

main contribution to the magnetic anisotropy. Moreover, the evaluated magnetic anisotropy constants of Co_{2c} and Co_{3g} sublattices using the experimental K_1 values showed that the local anisotropy constant of Co_{2c} is larger than that of Co_{3g} in CeCo₅. In the present work we show that Cu more effectively reduces the total magnetization when it occupies the 2c sites by suppressing the magnetic interaction within the Ce-Co_{2c} atomic layer and between the Co_{2c}-Co_{3g} layer. Therefore, at high temperatures, Cu doping at different Wyckoff positions shows contrasting impacts on the magnetization, as well as the magnetic anisotropy of Co sublattices, in which the Cu doping at the 3g sites is expected to give rise to larger magnetic anisotropy [68]. In practice, Cu is statistically distributed among the 2c and 3g sites [16] and the change of magnetic anisotropy with Cu content shows a nonmonotonic behavior, where the magnetic anisotropy maximum corresponds to the Cu content of approximately 20 at. % [16]. In the present work we do not consider Cu substitution of lower concentration, as for the simulation of Ce(Co_{1-x}Cu_x)₅ alloys with lower Cu content than 20 at. %, a larger supercell and thus much higher computational cost will be needed. Nevertheless, the existing maximum of the magnetic anisotropy as a function of Cu doping content can be understood from the point of view that with increasing Cu content, the contrasting impacts of the Cu substitutions at the 2c and 3g sites on the magnetic anisotropy would reach a counterbalance.

V. CONCLUSIONS

In conclusion, we carry out detailed investigations on the magnetic moments of Ce-4f and Co-3d shells, as well as the electronic structures of CeCo₅ and Ce(Co_{0.8}Cu_{0.2})₅ systems using the DFT + DMFT approach. Using CTQMC as impurity solver, we are also able to evaluate the Ce-4f valence fluctuations. The Coulomb U and J values of Co are determined using YCo₅ as a reference system. Subsequently, the magnetization as a function of temperature is calculated and the Curie temperatures at the mean-field level are obtained for YCo₅ and CeCo₅. According to the calculated electronic structure using both the DFT and DFT + DMFT methods, we find that the inclusion of dynamic correlation effects in Co-3d orbitals broadens the spectra, especially of the majority spin channel. Regarding the CeCo₅, the electronic structure of the Ce-4f states obtained from the DFT + DMFT method shows consistent energy positions of the 4f⁰, 4f¹, and 4f² configurations with experimental XPS and BIS spectra. The distribution probabilities of Ce-4f occupancy numbers are also given for CeCo₅, CeCo₄Cu_{2c}, and CeCo₄Cu_{3g} systems. We find that the addition of Cu slightly lowers the probability of $N = 0$ occupancy state, indicating a tendency to form a purely Ce³⁺ valence state. More interestingly, it is found that when Cu occupies the 2c sites, it imposes a stronger screening effect on the Ce-4f shell as compared to the 3g-sites doping, resulting in an almost vanishing total magnetic moment of CeCo₄Cu_{2c}. By contrast, the Ce-4f moment is slightly increased in CeCo₄Cu_{3g}. We thus suggest that the contrasting effects of Cu doping at the 2c and 3g sites on the magnetic properties of both Ce-4f and Co-3d states result in the non-monotonic change of the magnetic anisotropy as a function of Cu content in Ce(Co_{1-x}Cu_x)₅ alloys.

ACKNOWLEDGMENTS

We appreciate the funding by Deutsche Forschungsgemeinschaft (DFG, German Research Foundation) - Project-ID

405553726 - TRR 270. The Lichtenberg high-performance computer of TU Darmstadt is gratefully acknowledged for providing computational resources for all the calculations carried out in this work.

- [1] O. Gutfleisch, M. A. Willard, E. Brück, C. H. Chen, S. Sankar, and J. P. Liu, Magnetic materials and devices for the 21st century: Stronger, lighter, and more energy efficient, *Adv. Mater.* **23**, 821 (2011).
- [2] J. Coey, Hard magnetic materials: A perspective, *IEEE Trans. Magn.* **47**, 4671 (2011).
- [3] R. Skomski and D. Sellmyer, Anisotropy of rare-earth magnets, *J. Rare Earths* **27**, 675 (2009).
- [4] M. Kuz'min and A. Tishin, Chapter Three: Theory of crystal-field effects in $3d-4f$ intermetallic compounds, *Handbook Magn. Mater.* **17**, 149 (2007).
- [5] I. Campbell, Indirect exchange for rare earths in metals, *J. Phys. F* **2**, L47 (1972).
- [6] M. Richter, Band structure theory of magnetism in $3d-4f$ compounds, *J. Phys. D* **31**, 1017 (1998).
- [7] C. E. Patrick, S. Kumar, G. Balakrishnan, R. S. Edwards, M. R. Lees, L. Petit, and J. B. Staunton, Calculating the Magnetic Anisotropy of Rare-Earth-Transition-Metal Ferrimagnets, *Phys. Rev. Lett.* **120**, 097202 (2018).
- [8] H. Zhang, High-throughput design of magnetic materials, *Electron. Struct.* **3**, 033001 (2021).
- [9] H. Kirchmayr and C. Poldy, *Handbook on the Physics and Chemistry of Rare Earth*, edited by Gschneidner and Eyring (Elsevier, 1979).
- [10] L. Nordström, O. Eriksson, M. S. S. Brooks, and B. Johansson, Theory of ferromagnetism in CeCo_5 , *Phys. Rev. B* **41**, 9111 (1990).
- [11] C. E. Patrick and J. B. Staunton, Rare-earth/transition-metal magnets at finite temperature: Self-interaction-corrected relativistic density functional theory in the disordered local moment picture, *Phys. Rev. B* **97**, 224415 (2018).
- [12] V. Zepf, *Rare Earth Elements: A New Approach to the Nexus of Supply, Demand and Use: Exemplified Along the Use of Neodymium in Permanent Magnets* (Springer Science & Business Media, New York, 2013).
- [13] D. Gignoux, F. Givord, R. Lemaire, H. Launois, and F. Sayetat, Valence state of cerium in the hexagonal CeM_5 compounds with the transition metals, *J. Phys. France* **43**, 173 (1982).
- [14] E. Bauer, E. Gratz, and C. Schmitzer, CeCu_5 : Another Kondo lattice showing magnetic order, *J. Magn. Magn. Mater.* **63**, 37 (1987).
- [15] D. Girodin, C. Allibert, F. Givord, and R. Lemaire, Phase equilibria in the CeCo_5 - CeCu_5 system and structural characterization of the $\text{Ce}(\text{Co}_{1-x}\text{Cu}_x)_5$ phases, *J. Less-Common Met.* **110**, 149 (1985).
- [16] T. N. Lamichhane, M. T. Onyszczyk, O. Palasyuk, S. Sharikadze, T. H. Kim, Q. Lin, M. J. Kramer, R. W. McCallum, A. L. Wysocki, M. C. Nguyen, V. P. Antropov, T. Pandey, D. Parker, S. L. Budko, P. C. Canfield, and A. Palasyuk, Single-crystal permanent magnets: Extraordinary magnetic behavior in the Ta-, Cu-, and Fe-substituted CeCo_5 systems, *Phys. Rev. Appl.* **11**, 014052 (2019).
- [17] H. Shishido, T. Ueno, K. Saito, M. Sawada, and M. Matsumoto, Intrinsic coercivity induced by valence fluctuations in $4f-3d$ intermetallic magnets, [arXiv:2103.10202](https://arxiv.org/abs/2103.10202).
- [18] M. Croft, R. Neifeld, C. U. Segre, S. Raaen, and R. D. Parks, Ce valence variation in intermetallic alloys: L III absorption spectroscopy results, *Phys. Rev. B* **30**, 4164 (1984).
- [19] S. Sharma, E. Hildebrandt, M. Major, P. Komissinskiy, I. Radulov, and L. Alff, CeCo_5 thin films with perpendicular anisotropy grown by molecular beam epitaxy, *J. Magn. Magn. Mater.* **452**, 80 (2018).
- [20] K. Stevens, Matrix elements and operator equivalents connected with the magnetic properties of rare earth ions, *Proc. Phys. Soc. Sect. A* **65**, 209 (1952).
- [21] M. T. Hutchings, Point-charge calculations of energy levels of magnetic ions in crystalline electric fields, in *Solid State Physics* (Elsevier, Amsterdam, 1964), Vol. 16, pp. 227–273.
- [22] T. Miyake and H. Akai, Quantum theory of rare-earth magnets, *J. Phys. Soc. Jpn.* **87**, 041009 (2018).
- [23] Q. Si and S. Paschen, Quantum phase transitions in heavy fermion metals and Kondo insulators, *Phys. Status Solidi B* **250**, 425 (2013).
- [24] M. Klein, A. Nuber, F. Reinert, J. Kroha, O. Stockert, and H. v. Löhneysen, Signature of Quantum Criticality in Photoemission Spectroscopy, *Phys. Rev. Lett.* **101**, 266404 (2008).
- [25] T. Konishi, K. Morikawa, K. Kobayashi, T. Mizokawa, A. Fujimori, K. Mamiya, F. Iga, H. Kawanaka, Y. Nishihara, A. Delin *et al.*, Electronic structure of the strongly hybridized ferromagnet CeFe_2 , *Phys. Rev. B* **62**, 14304 (2000).
- [26] J. Herbst, $\text{R}_2\text{Fe}_{14}\text{B}$ materials: Intrinsic properties and technological aspects, *Rev. Mod. Phys.* **63**, 819 (1991).
- [27] M. Bartashevich, T. Goto, R. Radwanski, and A. Korolyov, Magnetic anisotropy and high-field magnetization process of CeCo_5 , *J. Magn. Magn. Mater.* **131**, 61 (1994).
- [28] M. Brooks, L. Nordstrom, and B. Johansson, $3d-5d$ band magnetism in rare earth-transition metal intermetallics: Total and partial magnetic moments of the RFe_2 ($\text{R} = \text{Gd-Yb}$) Laves phase compounds, *J. Phys.: Condens. Matter* **3**, 2357 (1991).
- [29] T. A. Butcher, W. Körner, G. Krugel, and C. Elsässer, Dependence of magnetisation and magnetocrystalline anisotropy on site distribution of alloying elements in RE-TM phases with ThMn_{12} structure, *J. Magn. Magn. Mater.* **441**, 1 (2017).
- [30] M. Lüders, A. Ernst, M. Däne, Z. Szotek, A. Svane, D. Ködderitzsch, W. Hergert, B. L. Györfly, and W. M. Temmerman, Self-interaction correction in multiple scattering theory, *Phys. Rev. B* **71**, 205109 (2005).
- [31] V. I. Anisimov, F. Aryasetiawan, and A. Lichtenstein, First-principles calculations of the electronic structure and spectra of strongly correlated systems: The LDA + U method, *J. Phys.: Condens. Matter* **9**, 767 (1997).
- [32] G. Kotliar, S. Y. Savrasov, K. Haule, V. S. Oudovenko, O. Parcollet, and C. A. Marianetti, Electronic structure calculations

- with dynamical mean-field theory, *Rev. Mod. Phys.* **78**, 865 (2006).
- [33] A. Galler, S. Ener, F. Maccari, I. Dirba, K. P. Skokov, O. Gutfleisch, S. Biermann, and L. V. Pourovskii, Intrinsically weak magnetic anisotropy of cerium in potential hard-magnetic intermetallics, *npj Quantum Mater.* **6**, 2 (2021).
- [34] P. Delange, S. Biermann, T. Miyake, and L. Pourovskii, Crystal-field splittings in rare-earth-based hard magnets: An *ab initio* approach, *Phys. Rev. B* **96**, 155132 (2017).
- [35] K. Haule, Quantum Monte Carlo impurity solver for cluster dynamical mean-field theory and electronic structure calculations with adjustable cluster base, *Phys. Rev. B* **75**, 155113 (2007).
- [36] K. Haule and T. Birol, Free Energy from Stationary Implementation of the DFT + DMFT Functional, *Phys. Rev. Lett.* **115**, 256402 (2015).
- [37] K. Haule, C.-H. Yee, and K. Kim, Dynamical mean-field theory within the full-potential methods: Electronic structure of CeIrIn₅, CeCoIn₅, and CeRhIn₅, *Phys. Rev. B* **81**, 195107 (2010).
- [38] K. Haule, <http://hauleweb.rutgers.edu/tutorials/>.
- [39] See the Supplemental Material at <http://link.aps.org/supplemental/10.1103/PhysRevB.106.224411> for justifications of the current methodology and extended results.
- [40] K. Haule, V. Oudovenko, S. Y. Savrasov, and G. Kotliar, The $\alpha\gamma$ Transition in Ce: A Theoretical View from Optical Spectroscopy, *Phys. Rev. Lett.* **94**, 036401 (2005).
- [41] B. Chakrabarti, M. E. Pezzoli, G. Sordi, K. Haule, and G. Kotliar, α - γ transition in cerium: Magnetic form factor and dynamic magnetic susceptibility in dynamical mean-field theory, *Phys. Rev. B* **89**, 125113 (2014).
- [42] P. Blaha, K. Schwarz, G. K. Madsen, D. Kvasnicka, J. Luitz *et al.*, WIEN2k, *An augmented plane wave + local orbitals program for calculating crystal properties* (Technische Universität Wien, 2001).
- [43] J. P. Perdew, K. Burke, and M. Ernzerhof, Generalized Gradient Approximation Made Simple, *Phys. Rev. Lett.* **77**, 3865 (1996).
- [44] K. Haule, Exact Double Counting in Combining the Dynamical Mean Field Theory and the Density Functional Theory, *Phys. Rev. Lett.* **115**, 196403 (2015).
- [45] K. J. Buschow, *Handbook of Magnetic Materials* (Elsevier, Amsterdam, 2003).
- [46] J. Schweizer and F. Tasset, Polarised neutron study of the RCo₅ intermetallic compounds. I. The cobalt magnetisation in YCo₅, *J. Phys. F* **10**, 2799 (1980).
- [47] C. E. Patrick, S. Kumar, G. Balakrishnan, R. S. Edwards, M. R. Lees, E. Mendive-Tapia, L. Petit, and J. B. Staunton, Rare-earth/transition-metal magnetic interactions in pristine and (Ni, Fe)-doped YCo₅ and GdCo₅, *Phys. Rev. Mater.* **1**, 024411 (2017).
- [48] J. Minár, Correlation effects in transition metals and their alloys studied using the fully self-consistent KKR-based LSDA + DMFT scheme, *J. Phys.: Condens. Matter* **23**, 253201 (2011).
- [49] M. Matsumoto, R. Banerjee, and J. B. Staunton, Improvement of magnetic hardness at finite temperatures: *Ab initio* disordered local-moment approach for YCo₅, *Phys. Rev. B* **90**, 054421 (2014).
- [50] E. Burzo, P. Vlačić, D. Kozlenko, N. Golosova, S. Kichanov, B. Savenko, A. Ostlin, and L. Chioncel, Structure and magnetic properties of YCo₅ compound at high pressures, *J. Mater. Sci. Technol.* **42**, 106 (2020).
- [51] J. Sánchez-Barriga, J. Braun, J. Minár, I. Di Marco, A. Varykhalov, O. Rader, V. Boni, V. Bellini, F. Manghi, H. Ebert *et al.*, Effects of spin-dependent quasiparticle renormalization in Fe, Co, and Ni photoemission spectra: An experimental and theoretical study, *Phys. Rev. B* **85**, 205109 (2012).
- [52] K. Buschow, Intermetallic compounds of rare-earth and 3d transition metals, *Rep. Prog. Phys.* **40**, 1179 (1977).
- [53] Q. Han, T. Birol, and K. Haule, Phonon Softening due to Melting of the Ferromagnetic Order in Elemental Iron, *Phys. Rev. Lett.* **120**, 187203 (2018).
- [54] A. S. Belozеров, I. Leonov, and V. I. Anisimov, Magnetism of iron and nickel from rotationally invariant Hirsch-Fye quantum Monte Carlo calculations, *Phys. Rev. B* **87**, 125138 (2013).
- [55] O. Zarechnyuk, R. Rikhal, and V. Koryin, X-ray study of the cerium-cobalt-aluminium ternary system alloys in the range of 0-33.3 at% of cerium, *Dopovidi Akademii Nauk Ukrain's' koj RSR. Seriya A, Fiziko-Tekhnichni ta Matematichni Nauki* **13**, 84 (1980).
- [56] I. L. M. Locht, Y. O. Kvashnin, D. C. M. Rodrigues, M. Pereiro, A. Bergman, L. Bergqvist, A. I. Lichtenstein, M. I. Katsnelson, A. Delin, A. B. Klautau, B. Johansson, I. DiMarco, and O. Eriksson, Standard model of the rare earths analyzed from the Hubbard I approximation, *Phys. Rev. B* **94**, 085137 (2016).
- [57] L. X. Benedict, D. Aberg, P. Soderlind, B. Sadigh, and M. Daene, Search for a consistent mean-field treatment of magnetic properties of YCo₅ under moderate hydrostatic stress Report No. LLNL-TR-678582, Lawrence Livermore National Laboratory, 2015.
- [58] O. Eriksson, M. S. S. Brooks, and B. Johansson, Orbital polarization in narrow-band systems: Application to volume collapses in light lanthanides, *Phys. Rev. B* **41**, 7311 (1990).
- [59] R. K. Chouhan and D. Paudyal, Cu substituted CeCo₅: New optimal permanent magnetic material with reduced criticality, *J. Alloys Compd.* **723**, 208 (2017).
- [60] S. Imada, S. Suga, T. Sato, R. Jung, and H. Ido, Electronic and magnetic states of RCo_{5-x}B_x investigated by photoemission and soft X-ray MCD, *J. Magn. Magn. Mater.* **226**, 1193 (2001).
- [61] F. U. Hillebrecht, J. C. Fuggle, G. A. Sawatzky, M. Campagna, O. Gunnarsson, and K. Schönhammer, Transition to non-magnetic f states in Ce intermetallic compounds studied by bremsstrahlung isochromat spectroscopy, *Phys. Rev. B* **30**, 1777 (1984).
- [62] J. Shim, K. Haule, and G. Kotliar, Fluctuating valence in a correlated solid and the anomalous properties of δ -plutonium, *Nature (London)* **446**, 513 (2007).
- [63] M. Janoschek, P. Das, B. Chakrabarti, D. L. Abernathy, M. D. Lumsden, J. M. Lawrence, J. D. Thompson, G. H. Lander, J. N. Mitchell, S. Richmond *et al.*, The valence-fluctuating ground state of plutonium, *Sci. Adv.* **1**, e1500188 (2015).
- [64] H. Lu and L. Huang, Electronic correlations in cerium's high-pressure phases, *J. Phys.: Condens. Matter* **30**, 395601 (2018).
- [65] J. C. Fuggle, F. U. Hillebrecht, Z. Zołnierek, R. Lässer, C. Freiburg, O. Gunnarsson, and K. Schönhammer, Electronic structure of Ce and its intermetallic compounds, *Phys. Rev. B* **27**, 7330 (1983).
- [66] D. Givord, J. Laforest, R. Lemaire, and Q. Lu, Cobalt magnetism in RCo₅-intermetallics: Onset of 3d magnetism and magnetocrystalline anisotropy (R = Rare earth or Th), *J. Magn. Magn. Mater.* **31**, 191 (1983).

- [67] M. Bartashevich, T. Goto, A. Korolyov, and A. Ermolenko, Co metamagnetism and magnetic anisotropy in single-crystalline $\text{Ce}(\text{Co}_{1-x}\text{Ni}_x)_5$, *J. Magn. Magn. Mater.* **163**, 199 (1996).
- [68] R. Choudhary, A. Palasyuk, I. C. Nlebedim, R. T. Ott, and D. Paudyal, Atomic cooperation in enhancing magnetism:(Fe, Cu)-doped CeCo_5 , *J. Alloys Compd.* **839**, 155549 (2020).
- [69] A. Ermolenko, Exchange interactions and magnetocrystalline anisotropy of rare earth-cobalt compounds with CaCu_5 -type structure, *IEEE Trans. Magn.* **15**, 1765 (1979).
- [70] C. E. Patrick and J. B. Staunton, Temperature-dependent magnetocrystalline anisotropy of rare earth/transition metal permanent magnets from first principles: The light RCo_5 ($\text{R} = \text{Y, La-Gd}$) intermetallics, *Phys. Rev. Mater.* **3**, 101401(R) (2019).
- [71] J.-X. Zhu, M. Janoschek, R. Rosenberg, F. Ronning, J. D. Thompson, M. A. Torrez, E. D. Bauer, and C. D. Batista, LDA + DMFT Approach to Magnetocrystalline Anisotropy of Strong Magnets, *Phys. Rev. X* **4**, 021027 (2014).
- [72] S. K. Panda, I. Di Marco, A. Delin, and O. Eriksson, Correlated electronic structure of CeN , *J. Electron Spectrosc. Relat. Phenom.* **208**, 111 (2016).
- [73] H. Okumura, T. Fukushima, H. Akai, and M. Ogura, First-principles calculation of magnetocrystalline anisotropy of $\text{Y}(\text{Co, Fe, Ni, Cu})_5$ based on full-potential KKR green's function method, [arXiv:2204.07384](https://arxiv.org/abs/2204.07384).